

Design and simulation of a wire scanner for the CSNS linac

RUAN Yu-Fang(阮玉芳)¹⁾ HAN Lu-Xiang(韩路祥) LIU Hua-Chang(刘华昌)
ZHANG Hua-Shun(张华顺) XU Tao-Guang(徐韬光) FU Shi-Nian(傅世年)

Institute of High Energy Physics, CAS, Beijing 100049, China

Abstract In this paper, we report the design and simulation of a wire scanner for the linac of the CSNS (China Spallation Neutron Source). The wire scanner is used to measure the transverse beam profile and the emittance. The effect of beam energy change upon the mechanical design of the wire scanner must be considered. The simulation results of heat on the two specified wires, tungsten and carbon, by using the finite element method software, ANSYS, are presented. In addition, the effect of wire deformation on the beam profile measurement is qualitatively analyzed, and the signal level of the wire scanner is discussed.

Key words CSNS, linac, wire scanner

PACS 29.20.Ej

1 Introduction

The China Spallation Neutron Source project (CSNS) [1] is an accelerator-based high power project currently under R&D in China. The accelerator complex consists of an 81 MeV H^- linear accelerator as the injector and a 1.6 GeV rapid cycling proton synchrotron (RCS). The linear accelerator consists of a 50 keV H^- Penning surface plasma ion source, a low beam energy transport line (LEBT), a 3 MeV Radio Frequency Quadrupole (RFQ) accelerator, a Medium Energy Beam Transport line (MEBT), an 81 MeV Drift Tube Linear Accelerator (DTL) and a Linac to Ring Beam Transport (LRBT). For CSNS Phase-II, the energy at the exit of the DTL will be 132 MeV. The major parameters of the CSNS Linac are listed in Table 1. One of the beam instruments being developed for CSNS commissioning is a wire scanner,

which is used to measure the beam profile. A beam profile measurement is important to control the beam width, as well as the transverse matching between different parts of an acceleration facility. The locations of the wire scanners are shown in Fig. 1. At the LRBT, it is planned to use multi-WS for beam emittance measurements. Note that the wire scanners used after the DTL tanks will be removed after the DTL installation is completed.

Table 1. The major parameters of the CSNS linac.

ion	H^-
kinetic energy	3–132.2 MeV
pulse current	0.5–30 mA
repetition rate	25 Hz
RF frequency	324 MHz
RMS beam size	0.9–2 mm

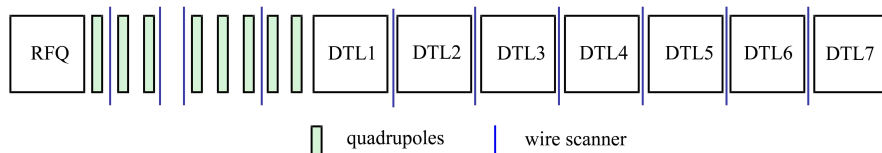


Fig. 1. Schematic layout of wire scanners in the CSNS linac.

Received 11 November 2009

1) E-mail: ruanyf@ihep.ac.cn

©2010 Chinese Physical Society and the Institute of High Energy Physics of the Chinese Academy of Sciences and the Institute of Modern Physics of the Chinese Academy of Sciences and IOP Publishing Ltd

2 Mechanical designs

The mechanical model of the wire scanner is shown in Fig. 2. The wire scanner will be mounted at 45° to the horizontal plane. The outer assembly that resides outside the vacuum consists of a stepper motor, a linear encoder and an electric control platform. The inner assembly consists of a movable frame that carries three sensing wires.

Based on the experience of SNS and LEDA, the clamp grasping the wire is chosen, as shown in Fig. 3. The structure of the clamp can solve the problem of

wire sagging and electrical isolation. The signal from the sensing wire will be measured, therefore the wire clamp needs electrical isolation by using a ceramic block. The retaining ring will be used to prevent the collet from slipping off. Once the spring is compressed, the collar will press the collet, otherwise the wire will be moveable.

Based on the experience of SNS [2], LEDA [3] and J-PARC [4], two wire types are considered: tungsten and carbon. The properties of the two wires are listed in Table 2. The 32 micron diameter carbon wire is selected for use. For the tungsten wire, we investigate 25 micron diameter wire.

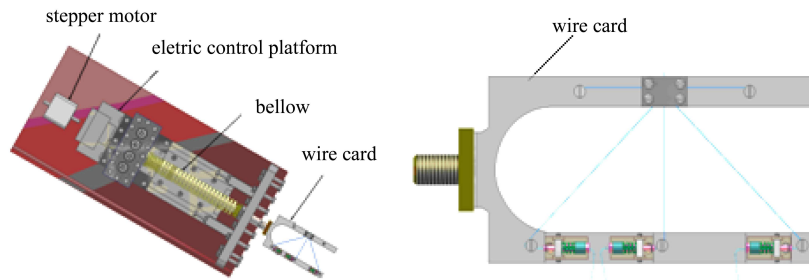


Fig. 2. The mechanical model of the wire scanner.

Table 2. The properties of carbon and tungsten.

material	density/ (kg/m^3)	melting point/K	thermal conductivity/($\text{W}/\text{K}/\text{m}$)	radiant emissivity	special heat/($\text{J}/\text{kg}/\text{K}$)	tensile strength/ MPa
carbon	2000	3870	24	0.8	752	430
tungsten	19350	3700	130	0.13	150	3000

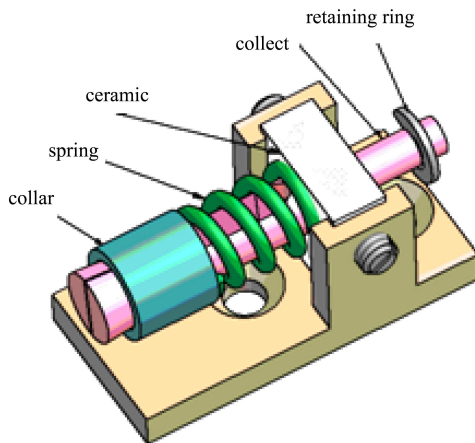


Fig. 3. The wire clamp.

3 Thermal analysis results

The sensing wires of the wire scanner will intercept the beam as they move through it, and the en-

ergy deposited in the wire will cause a temperature increase. In the worst case, the temperature is so high that it could cause the wires to melt. Therefore, the goals of designing the wire are determining the maximal temperature of the wire during the scan and the beam parameter range that is safe for operation of the wire scanner. The temperature of a wire is decided by heating the wire with the beam and then using three cooling mechanisms: radiant cooling, heat conduction along the wire and thermionic cooling. Since the heat conduction and thermionic cooling are small compared with the radiant cooling, the value of the wire temperature can be mainly deduced by the heating of the wire by the beam and radiant cooling.

When a H^- beam enters a thin wire, the two loosely bound electrons quickly detach from the proton, resulting in three independent charged particles, each contributing to the energy loss of the beam in the wire. The energy losses of protons and electrons are listed in Table 3.

Table 3. The energy loss of two types of wires vs. variable beam energy.

position	beam energy/MeV	32 μm carbon wire		25 μm tungsten wire	
		proton energy	single electron	proton energy	single electron
		loss/MeV	energy loss/MeV	loss/MeV	energy loss/MeV
MEBT	3	0.66	0.0016	1.42	0.0016
DTL 1	21.76	0.138	0.012	0.41	0.012
DTL 2	41.65	0.082	0.022	0.26	0.022
DTL 3	61.28	0.061	0.033	0.197	0.033
DTL 4	80.77	0.048	0.044	0.16	0.044
DTL 5	98.86	0.042	0.054	0.142	0.054
DTL 6	115.8	0.037	0.063	0.127	0.063
DTL 7	132.2	0.034	0.029	0.116	0.072

It is clear from Table 3 that the energy loss of the electron is not negligible compared with that of the proton for the high beam energy exceeding 10 MeV. Note that the electron energy loss of the carbon wire is lower than that of the tungsten wire for beam energy 132.2 MeV, because the electrons exit from the carbon wire but they stop in the tungsten wire.

The total energy losses in the two wires versus beam energies are shown in Fig. 4.

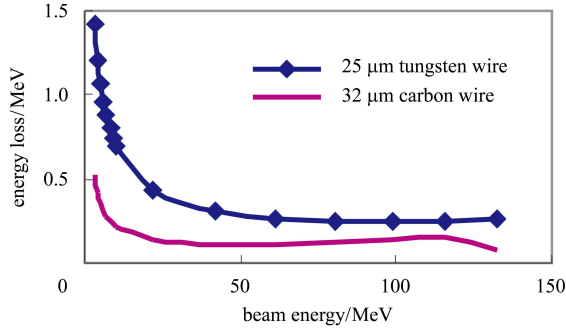


Fig. 4. The energy losses in the wires vs. beam energies.

Figure 4 shows that the deposit energy in the wire decreases with increasing beam energy. The energy loss in the 32 μm carbon wire is less than that in the 25 μm tungsten wire. From this point of view, the carbon wire is more suitable for the wire scanner.

The temperature variations in the wire can be deduced by the following governing equation [5],

$$\rho \frac{dE}{dx} I_{\text{peak}} V - \varepsilon \sigma (T^4 - T_{\text{surr}}^4) A_s - \lambda V \frac{d^2 T}{dy^2} = \rho V c_p \frac{dT}{dt}, \quad (1)$$

where ρ is wire material density (g/cm^3), $\frac{dE}{dx}$ is the stopping power ($\text{MeV} \cdot \text{cm}^2/\text{g}$), I_{peak} is the peak current of the beam ($\mu\text{A}/\text{cm}^2$), V is the volume of the

wire under consideration (cm^3), ε is the emissivity of the wire material, σ is the Stephan-Boltzmann coefficient ($5.67 \times 10^{-12} \text{ W}/\text{cm}^2/\text{K}^4$), T is the temperature of the wire (K), T_{surr} is the temperature of the surroundings (K), A_s is the surface area of the wire (cm^2), λ is the wire thermal conductivity ($\text{W}/\text{cm}/\text{K}$), $\frac{d^2 T}{dy^2}$ is the differential of the temperature gradient along the wire, c_p is the specific heat capacity of the wire material ($\text{J}/\text{g}/\text{K}$) and $\frac{dT}{dt}$ is the time rate of change of temperature (K/s).

The first term on the left hand side of Eq. (1) represents the energy generated inside the control volume. The second term represents the radiant cooling of the wire. The third term represents the wire cooling by heat transport. The term on the right hand side represents the energy stored inside the control volume.

The ANSYS software using finite element analysis (FEA) is used to deduce the peak temperatures of the two wires for the two beam conditions, as shown in Table 4. The beam current for the analysis is 30 mA. The wires are assumed to be in the center of the beam.

It is clear from Table 4 that the temperature of the tungsten wire is higher than that of the carbon wire due to its high density and low radiant emissivity. Because of the limited wire temperature of 1800 K [3], carbon wire can be used in MEBT for the beam condition of a 1 Hz repetition rate and a 50 μs pulse width rather than tungsten wire. For the higher beam energy, both carbon and tungsten wires can be used.

A numerical integration technique is used for Eq. (1) to determine the time rate of the change of temperature (dT/dt). Fig. 5 shows a typical plot of the temperature rise in a 32 μm carbon wire at a 50 μs pulse length and a 1 Hz beam repetition rate. It is obvious that the result of the finite element analysis is quite consistent with that of the numerical analysis.

Table 4. The peak temperatures of the two wires for the various beam conditions.

position	beam energy/MeV	x (RMS,cm)	y (RMS,cm)	32 μm carbon wire		25 μm tungsten	
				peak temp./K		wire peak temp./K	
				1Hz, 50 μs	1Hz, 100 μs	1Hz, 50 μs	1Hz, 100 μs
MEBT ⁰	3	0.086	0.129	1732	2805	–	–
DTL 1	21.76	0.1314	0.096	780	1101	2070	3593
DTL 2	41.65	0.115	0.1367	656	900	1386	2293
DTL 3	61.28	0.1208	0.1418	646	884	1201	1944
DTL 4	80.77	0.1643	0.1355	608	822	996	1563
DTL 5	98.86	0.1623	0.1396	631	857	991	1548
DTL 6	115.8	0.1663	0.1489	638	869.5	958	1484
DTL 7	132.2	0.1507	0.1656	505	660	970	1504

(0: the wire scanner after the first quadrupole magnets in MEBT. –: the temperature is out of the melting point of tungsten)

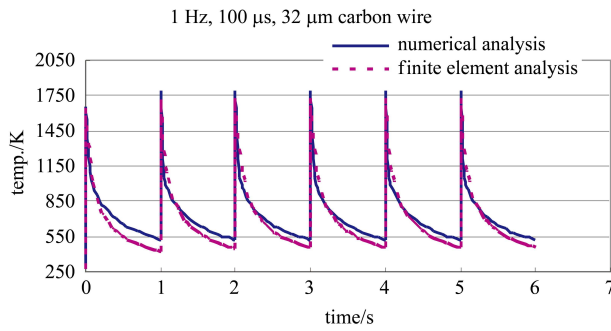


Fig. 5. Temperature rise in a 32 μm carbon wire by numerical analysis and finite element analysis.

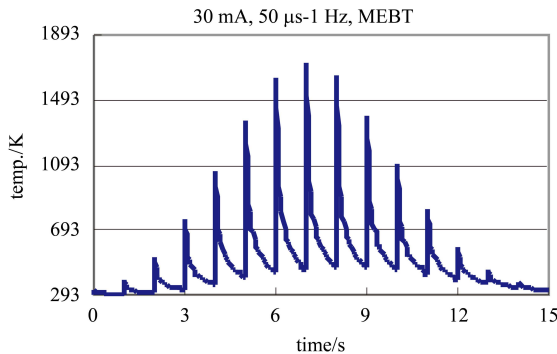


Fig. 6. The wire scans the whole beam profile via 15 pulse-steps.

The above discussion is based on a stationary wire, while the wire is used to scan the beam profile via pulse-steps. The maximum temperature of the wire is simulated by ANSYS, as shown in Fig. 6.

Figure 6 shows that the maximum temperature of the wire appears in the middle of the beam. The temperature should be strictly limited to below 1800 K.

4 The effect of the wire deformation

According to the thermal results of the two wires

mentioned above, the carbon wire is selected in MEBT. The tensile strength of the 30 μm carbon wire that we have purchased is 430 MPa, as shown in Table 2, and it could just stand the tension of ten grams. So it is so fragile to add pre-tensioning to the wire. Without pre-tensioning, the wire will sag caused by beam heating during its scanning. We also need to consider the effect on the beam profile measurement.

Figure 7 shows that the vertical profile of the beam is obtained by the horizontal wire. The effect of deformation of the wire on the vertical profile measurement is greatest.

Assuming that the cross-section of the beam is a 2D Gaussian distribution, the vertical beam profile can be deduced as

$$f(y) = \int_{-\frac{L}{2}}^{\frac{L}{2}} \frac{1}{2\pi\sigma^2} e^{-\frac{x^2}{2\sigma^2}} e^{-\frac{(y - \sqrt{R^2 - x^2} + \sqrt{R^2 - (\frac{L}{2})^2})^2}{2\sigma^2}} \times \frac{R}{\sqrt{R^2 - x^2}} dx, \quad (2)$$

where L is the original wire length without deformation, R is the radius of curvature of the wire after deformation and σ is the RMS beam size.

It can be deduced from Eq. (2) that the center of the beam profile will have an offset compared with that of the original beam profile, as shown in Fig. 7(b). The value of the offset is

$$R - \sqrt{R^2 - \left(\frac{L}{2}\right)^2}.$$

The above discussion is based on the fixed deformation of the wire, but Fig. 6 shows that the temperature of the wire is variable during scanning. Therefore the deformation of the wire is variable. The beam profile with variable deformation is shown in Fig. 8.

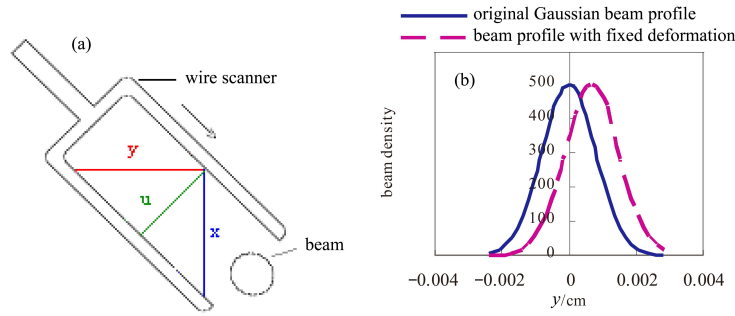


Fig. 7. (a) The display of how to measure the beam profile. (b) The vertical beam profile before and after deformation.

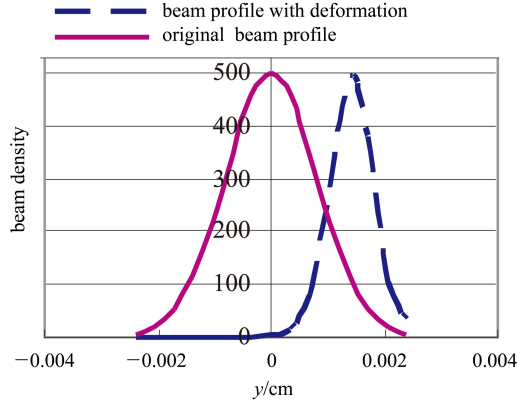


Fig. 8. The beam profile with variable deformation and original beam profile.

It can be qualitatively deduced from Fig. 8 that if the wire undergoes deformation, the RMS beam size with variable deformation will be smaller than its actual size.

Therefore, the wire does need to have pre-tensioning to prevent the wire from deforming. The key issue of how to add the pre-tensioning to the wire is being solved.

5 Signal levels of the wire scanners

Since H^- beams are accelerated in the linac of CSNS, there are four sources of the signal generated in a wire by collision of H^- beams: (1) positive current by the proton flowing into a beam, (2) negative current by the electron flowing into a beam, (3) positive current by secondary electron emission (SEM) when protons impact a wire and (4) positive current by thermal electron emission when the wire is heated.

For 32 μm carbon wire, when the beam energy $E=3\text{--}115.8$ MeV, protons penetrate the wire and electrons stop in the wire and the signals are generated by only the above mentioned (1), (3) and (4); when the beam energy $E=132.2$ MeV, protons and electrons penetrate the wire and the signals are generated by

only the above mentioned (3) and (4). For 25 μm tungsten wire, when $E=3\text{--}132.2$ MeV, the signals are generated by only the above mentioned (1), (3) and (4).

The thermionic emission from the hot wire is described by Richardson Dushman [6]. It can be deduced that the thermionic emission current that is also less than 1% of the SEM current can be ignored when the wire temperature is below 1800 K.

A well-known theory from Sternglass describes the secondary emission yield [7]. The relationship between the secondary emission yields of the two wires and variable beam energies are shown in Fig. 9.

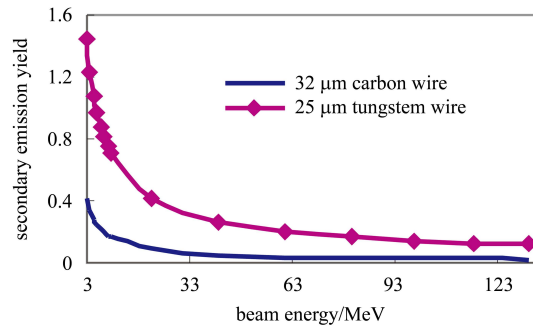


Fig. 9. The secondary emission yields of the two wires vs. variable beam energies.

Without considering the bias voltage applied to the wire, as a result, the total estimated signals of the wires are listed in Table 5.

Table 5 shows that for 32 μm carbon wire the Max. and Min. signals in the center of beam are about -0.765 mA and -0.228 mA, respectively, in CSNS Phase-I. The wires are used to probe the beam from its center to the approximate 3-RMS-width location, so the beam dynamic range is about 10^3 . Adding the beam current range from 5 mA to 30 mA, as a result, the total current range is -0.038 μA to -0.765 mA. For 25 μm tungsten wire, the total current range is -0.01 μA to -0.49 mA.

Table 5. The estimation of signals in the center of the beam, 30 mA Avg. beam current for two wires.

position	beam energy/MeV	RMS, Min./cm	32 μm carbon signal/mA	25 μm tungsten wire signal/mA	RMS, Max./cm	32 μm carbon signal/mA	25 μm tungsten wire signal/mA
MEBT	3	0.08	-0.7611	-0.20825	0.267	-0.2283	-0.06247
DTL 1	21.76	0.096	-0.7653	-0.49499	0.131	-0.5591	-0.36164
DTL 2	41.65	0.115	-0.6507	-0.45291	0.137	-0.5474	-0.38101
DTL 3	61.28	0.121	-0.6237	-0.44672	0.142	-0.5313	-0.38056
DTL 4	80.77	0.135	-0.5581	-0.40607	0.164	-0.4603	-0.33489
DTL 5	98.86	0.139	-0.5429	-0.3988	0.162	-0.467	-0.34302
DTL 6	115.8	0.149	-0.5097	-0.37686	0.166	-0.4564	-0.33743
DTL 7	132.2	0.151	0.0054	-0.37454	0.166	0.0049	-0.34084

It is clear that the current range is so large that it imposes strong demands on the electronics system. To solve this problem, we will use different electronics for different positions.

6 Conclusion

The mechanical design of the wire scanners for CSNS is described. Based on the experience of SNS and LEDA, the clamp that can solve the problem of wire sagging and electrical isolation is chosen. The results of the thermal analysis of the carbon and tungsten wires indicate that the carbon wire is more suitable at low beam energy (~ 3 MeV) and both wires are suitable at high beam energy, because the deposited

energy in the wire decreases with an increase in the beam energy.

For carbon wire, it is hard to add pre-tensioning. Without pre-tensioning, the wire deformation can affect the beam profile center and its RMS beam size. Therefore, the wire does need to have pre-tensioning during scanning. The key issue of how to add the pre-tensioning to the wire is being solved.

The current range of carbon wire is larger than that of tungsten wire and it will make strong demands on the electronics system. Therefore, both wires have their advantages and disadvantages. As a result, the carbon wire will be selected at the location of MEBT, and the tungsten wire will be used for the higher beam energy.

References

- 1 WEI J et al. Nucl. Instrum. Methods A, 2009, **600**: 10–13
- 2 Michael Plum. LANL Wire Scanner Final Design Review. <http://neutrons.ornl.gov/diagnostics/papers>
- 3 Valdiviez R et al. Proceedings of the Particle Accelerator Conference. American: Chicago, 2001. 1324–1326
- 4 Akikawa H et al. Linear Accelerator Conference. American: Tennessee, 2006. 293–295
- 5 Liaw C J et al. Proceedings of the Particle Accelerator Conference. American: Chicago, 2001. 2365–2367
- 6 Mariusz Sapinski. Model of Carbon Wire Heating in Accelerator Beam, CERN-AB-2008-030-BI, July 2008
- 7 Sternglass E J. Phys. Rev., 1957, **1**: 108